Chelator-impregnated polydimethylsiloxane beads for the separation of medical radionuclides

Santoso, Albert; Trapp, Svenja; Blommestein, Iris M.S.; Saedy, Saeed; van Ommen, J. Ruud; de Kruijff, Robin M.; van Steijn, Volkert

DOI
10.1016/j.seppur.2024.128865

Publication date
2025

Document Version
Final published version

Published in
Separation and Purification Technology

Separation and Purification Technology 354 (2025) 128865

Contents lists available at ScienceDirect

Separation and Purification Technology

journal homepage: www.elsevier.com/locate/seppur

Chelator-impregnated polydimethylsiloxane beads for the separation of medical radionuclides

Albert Santoso [a,1], Svenja Trapp [b,1], Iris M.S. Blommestein [a], Saeed Saedy [a], J. Ruud van Ommen [a], Robin M. de Kruijff [b,*], Volkert van Steijn [a,*]

[a] Department of Chemical Engineering, Delft University of Technology, Van der Maasweg 9, Delft, 2629 HZ, The Netherlands
[b] Department of Radiation Science and Technology, Delft University of Technology, Mekelweg 15, Delft, 2629 JB, The Netherlands

ARTICLE INFO

Keywords:
Chelator-impregnated resin
Radionuclide separation
Medical radionuclides
Ac-225
PDMS

ABSTRACT

Chelator-impregnated resins have been studied earlier for the chemical separation of elements in aqueous solutions, but issues with their chemical stability have limited their use in the separation of (medical) radionuclides from their respective irradiated targets. We developed a polydimethylsiloxane (PDMS)-based chelator-impregnated resin that showed a high chemical stability against leaching. Several different chelators were tested in this study. After impregnation of the PDMS beads with the di-2-ethylhexylphosphoric acid (D2EHPA) chelator, an in-flow separation study with various radionuclides (Y-90, La-140, and Ac-225) was conducted. These three radionuclides have potential use in nuclear medicine and a production route through irradiation of Sr-, Ba-, and Ra-targets respectively, necessitating their chemical separation. The D2EHPA-impregnated beads achieved high adsorption efficiencies of 99.89% ± 0.14%, 99.50% ± 0.10%, and 98.51% ± 0.25%, for Y-90, La-140, and Ac-225, respectively, while co-adsorption of minor amounts (< 3%) of the targets were reported. These results, together with the high chemical stability of the PDMS-based resin, highlight the potential of chelator-impregnated resins in the rapidly growing field of (medical) radionuclide production.

1. Introduction

In the field of nuclear medicine, antibodies, peptides, or small molecules labelled with radionuclides are used for nuclear imaging of a malignancy, or for the delivery of a therapeutic radiation dose to a specific tumor site while minimizing the dose to surrounding healthy tissue [1,2]. For decades, just a few radionuclides have been used in clinical settings, including the positron (β^+) emitters Ga-68 and F-18 for positron emission tomography (PET) [3,4], the gamma (γ) emitter Tc-99 m for single-photon emission computed tomography (SPECT) [4], and the alpha (α) emitter Ra-223 for the treatment of bone metastases [5]. With technological advancements in targetry and irradiation facilities, increasing numbers of radionuclides are researched for their potential use in nuclear medicine to maximize worldwide capacity and availability of medical radionuclides [1,2,6]. Yet, few make it to clinical applications [1,2,6,7].

One of the biggest challenges in realizing the full potential of these radionuclides lies in the production steps and the availability of the enriched target material needed for the production [7]. Most medical radionuclides are produced by irradiation of costly, enriched target materials, either as solid or liquid targets. After irradiation, the produced radionuclide is separated from its respective target and the target material is recovered to be re-used. This separation should be performed quickly, especially in the case of short-lived radionuclides (e.g., Ga-68 with a half-life of $t_{1/2}$ = 67.71 minutes). The separation should also result in a high chemical and radio chemical purity [8] for further use in radiopharmaceutical production. Moreover, concerns about good manufacturing practices (GMP), radiation safety, and cost necessitate a simple, automatable separation process [9,10].

The most common method for the chemical separation of a product radionuclide from its target is ion-exchange chromatography [11]. In ion-exchange chromatography, the separation of the radionuclide from its target material is commonly done by flowing an aqueous solution containing the product radionuclide and target material through a resin-packed column. The resin consists of a solid support with covalently bound functional (charged) groups. The functional groups act as a binding site, often adsorbing both the radionuclide and the target material. Hereafter, selective elution of the radionuclide, the target, and possible contaminants from the resin is done by subsequently flowing aqueous solutions with a different pH through the column. This also

* Corresponding authors.
E-mail addresses: a.santoso@tudelft.nl (A. Santoso), R.M.deKruijff@tudelft.nl (R.M. de Kruijff), V.vanSteijn@tudelft.nl (V. van Steijn).
[1] Shared first authorship.

https://doi.org/10.1016/j.seppur.2024.128865
Received 19 April 2024; Received in revised form 4 July 2024; Accepted 16 July 2024
Available online 20 July 2024

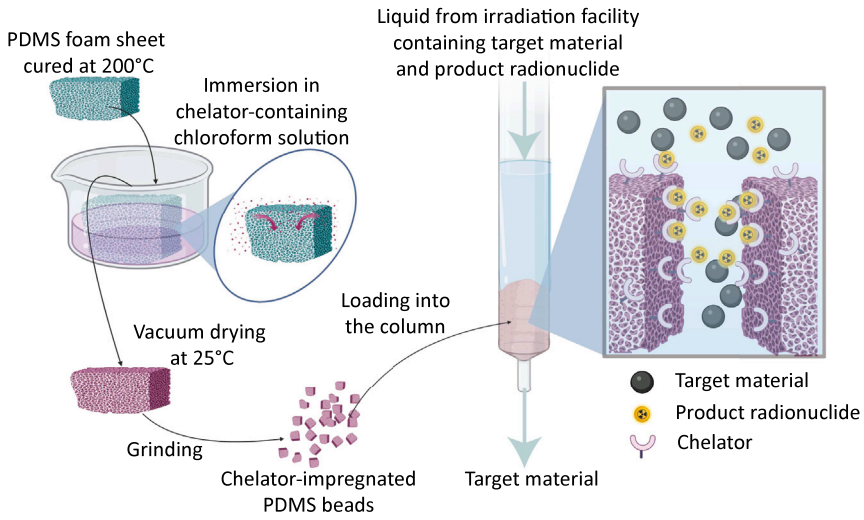

Fig. 1. Illustration of the fabrication of chelator-impregnated PDMS beads (left) and their use in separating a product radionuclide of interest from its target material (right). Cured PDMS foam sheets are immersed in a chelator-containing chloroform solution before being vacuum-dried and mechanically ground into beads. The chelator-impregnated PDMS beads are loaded into a flow column, through which liquid containing the product radionuclide of interest and its target is flown. The radionuclide selectively binds to the chelator on the beads, resulting in a separated target solution leaving the column. The radionuclide is subsequently collected by flowing an eluting solution with a specific pH through the column.

necessitates multiple processing steps to recycle the expensive enriched target material [12–16].

As an alternative to traditional ion-exchange resins, chelator-impregnated resins have been studied. In this approach, a chelator or extracting agent is impregnated onto polymer-based resin beads that act as the solid support [17]. Chelators can have a high selectivity towards the product radionuclide over its target material, forming stable coordination bonds [18]. Due to this high selectivity, a lower amount of resin, and, subsequently, lower volumes of chemicals are needed [19]. Additionally, chelator-impregnated resins possibly allow for direct recycling of the target when a liquid target is used [19], because the target is not adsorbed on the resin. Despite the potential advantages of chelator-impregnated resins, the chemical stability of the resins remains an issue. When in contact with acidic solutions, the chelator can be leached [20]. Consequently, the resins are no longer usable, the expensive target solution can no longer be recycled directly, and the chemical purity of the radionuclide solution decreases, posing issues with GMP production. To overcome this, a highly stable combination of support material, chelator, and impregnating method with selective adsorption towards the product radionuclide needs to be found [21].

In this paper, we present the synthesis and application of chelator-impregnated polydimethylsiloxane (PDMS) beads with high selectivity towards the radionuclide of interest and a high chemical stability against leaching, for the separation of selected medical radionuclides, as illustrated in Fig. 1 and detailed in Patent No. 203,7212 [22]. Unique when compared with other supporting materials used for chelator-impregnated resins, PDMS has a high resistance against acids, but swells upon contact with common organic solvents in which most chelators can be dissolved [23]. This allows the incorporation of a chelator inside the PDMS, before the PDMS shrinks back upon removal of the organic solvent [24], both physically trapping the chelator and hydrophobically binding it to the surface. This improves the chemical stability of the chelator-impregnated resin and subsequently prevents leaching of the chelator, a known problem in the applications of chelator-impregnated resins [21,25]. Making use of this feature of PDMS, we demonstrate the fabrication of chelator-impregnated PDMS beads for three different types of chelators: N-benzoyl-N-phenylhydroxylamine (BPHA), di-2-ethylhexylphosphoric acid (D2EHPA), and dithizone (DTZ), all dissolved in chloroform. The selection of the chelators was made due to their demonstrated applicability for the separation of the medical radionuclides Ac-225, Cu-64 [26,27], and Ga-68 [28], respectively. We subsequently demonstrate our concept with a case study using D2EHPA-impregnated PDMS beads for the separation of Yttrium and Lanthanum (both possessing medically interesting radionuclides such as the β^+ emitting Y-86 and La-132 [29,30]) from their respective Strontium and Barium targets, as well as Actinium from Radium, motivated by the increasing attention for the use of Ac-225 in targeted alpha therapy [31,32].

2. Methods and materials

2.1. Fabrication of chelator-impregnated PDMS beads

PDMS beads were fabricated by suspending the PDMS elastomer (dime-thylsiloxane, Sylgard 184 Elastomer Kit, Dow Corning) in water with a mass ratio of 1:5. The suspension was then mixed with a vortex mixer (Vortex Genie 2, Scientific Industries) for 10 minutes before a PDMS curing agent (methyl hydrosilane, Dow Corning) was added with a mass ratio of 1:2 to the elastomer. The mixture was then remixed with the vortex mixer for another 2 minutes before slowly being poured into a beaker containing 10 times as much water by weight at 100 °C. After pouring, an opaque solid foam-like sheet formed on the surface of the boiling water. This PDMS foam sheet was taken out and cured in an oven at 200 °C for at least 10 h.

Impregnation of the cured PDMS foam sheet with a chelator was done by immersing the sheet in a chloroform solution containing the dissolved chelator at a concentration ranging from 0.01 M to 0.75 M, depending on the solubility of the chelator used and its common practice [33–35]. Three different chelators were studied: N-benzoyl-N-phenylhydroxylamine (BPHA, > 98%, VWR), di-2-ethylhexylphosphoric acid (D2EHPA, > 98%, Merck Sigma), and 1-anilino-3-phenyliminothiourea (dithizone, DTZ, > 98%, Merck Sigma). After immersion for 10 h at 25 °C and atmospheric pressure in a container open to the atmosphere of a fume hood, the remaining chloroform was removed by placing the container in a vacuum desiccator ($\sim 10^{-2}$ mbar) for 30 minutes.

Chelator-impregnated PDMS beads were obtained by grinding the chelator-impregnated PDMS foam sheets in an electric coffee mill grinder (PCKSW 1021 N) for 5 minutes. Initial tests on bare PDMS beads were performed to determine the influence of the operating parameters of the grinder on the diameter of the beads, see Figure A.1. With the chosen operating parameters, the median diameter of the chelator-impregnated beads was 0.4 ± 0.1 mm.

2.2. Characterization of the PDMS beads

To characterize the diameter of the PDMS beads, brightfield images of the beads were recorded using a camera (ImagingSource DFK33UX273) mounted on an optical microscope (Oxion Inverso) through a 4x Plan Phase LWD Infinity Corrected IOS objective. The obtained images were processed using ImageJ software [36]. From the two-dimensional images, the median diameter of the beads was determined using Martin's diameter. Martin's diameter is defined as the maximum measured distance between opposite sides of the non-spherical beads and was measured transverse to the beads on a line that bisects the projected area [37]. The median diameter of the beads was obtained by measuring Martin's diameter of 100 beads. The PDMS bead diameter was used to obtain a conservative estimate of the available surface area of the PDMS beads.

The impregnation of the chelators was characterized using attenuated total reflection Fourier-transform infrared spectroscopy (ATR-FTIR, Thermo Nicolet NEXUS) with a wavelength range of 4000 to 500 cm^{-1}. To observe the surface structure of the chelator-impregnated PDMS beads, we conducted field emission scanning electron microscopy (FE-SEM, Hitachi Regulus SU8230) at a beam current of 1 μA and electron energy of 3–5 keV. To approximate the mass of the impregnated chelators in the PDMS beads, a thermogravimetric analysis (TGA, METTLER TOLEDO SF/1100) was performed by heating the beads to 800 °C at a rate of 10 °C min^{-1} under nitrogen (100 mL min^{-1}). Since PDMS starts degrading at temperature above 320 °C [38], while the chelators degrade at lower temperatures (200 °C to 300 °C for BPHA [39], 120 °C to 270 °C for D2EHPA [35,40], and 150 °C to 250 °C for DTZ [41]), the weight difference at 310 °C was used to approximate the chelator mass [40,42]. To gain insights on the impregnation mechanism, X-ray photoelectron spectroscopy (XPS, ThermoFisher Scientific Nexsa) was performed using an XPS spectrometer equipped with a monochromatic Al Kα radiation source and a pass energy of 30 eV for the survey scan. Since the XPS beam source and detector are placed at an angle, the XPS reading on particles with random shapes and relatively large sizes can be less reliable. We therefore performed the XPS measurements on a flat layer of PDMS, spin-coated on a silicon wafer [43], and immersed in the chelator-containing chloroform solution, following the method described before. A depth profiling was then conducted by etching the surface using Ar^+ ions (2 keV with a raster size of 1 mm) while the differential charging was compensated using a flood gun. CASA-XPS software was used to post-process the XPS peak profiles, where the spectra were charge-corrected with the adventitious carbon peak at 284.8 eV.

2.3. Chemical stability test of chelator-impregnated PDMS beads

We tested the stability of the impregnated beads in pure Milli-Q water and the following acidic solutions: 1 M HCl, 12 M HCl (ACS reagent 37%, Merck Sigma), and 1 M HNO_3 (65%, Merck Sigma). To this end, we immersed 0.5 g of the chelator-impregnated PDMS beads in 5 mL of the acidic solution in a 15 mL Falcon tube, which was continuously shaken (IKA Vibrax VX-2) for short (5 minutes) and long (8 h) immersion times. The beads were subsequently washed with pure Milli-Q water before being characterized using XPS. In addition, all immersion solutions were characterized using an ultraviolet–visible spectrophotometer (UV–Vis, NanoDrop 2000/2000c) with a wide scan reading (300–800 nm).

As a reference, we also tested the stability of chelator-impregnated silicon (IV) oxide powder (Silica, 99.5%, Millipore, 0.063–0.200 mm), where the powder was impregnated with the chelators following a similar methodology to the impregnation of PDMS beads. The chelator-impregnated silica powder was subsequently immersed in the same acidic solutions. Once the powder was separated, the immersion liquid was characterized using UV–Vis. Since the concentration of the chelators leached from the silica powder was higher than the concentration from the PDMS beads, the immersion liquid was diluted 1000 times before being measured with UV–Vis. Please note that the concentration of the leached BPHA and DTZ from silica powder after dilution was within the detection limit of the UV–Vis. However, the leached D2EHPA was in the liquid phase at room temperature. Due to its relatively high concentration, the leached D2EHPA from silica powder was highly dispersed in the immersion liquid, resulting in an opaque liquid. This high opacity reduced the reliability of UV–Vis measurement, even after being diluted 10^9 times. Therefore, to quantify the leached D2EHPA from the chelator-impregnated silica powder reliably, the opaque D2EHPA immersion liquid was left in the fume hood for 24 h to partition. After 24 h, two liquid phases separated and a clear boundary between the two phases was observed. The top liquid was decanted and the bottom liquid was weighed, indicating the mass of the leached D2EHPA.

To evaluate the interaction between the chelator and the PDMS responsible for the chemical stability (i.e., minimal leaching), the extended Derjaguin–Landau–Verwey–Overbeek theory (EDLVO) was used [44–51]. More specifically, we determined the Gibbs free energy, which is an indicator of the interaction strength between the chelator and the PDMS. The details of the calculation can be found in Supplementary Information.

2.4. Radiotracer production and radioactivity measurements

The radiotracers Y-90, La-140, and Cu-64 were produced by neutron irradiation of Y_2O_3, La_2O_3 (Merck Sigma), and Zn-foil, respectively, at the Hoger Onderwijs Reactor (HOR) of the TU Delft Reactor Institute, the Netherlands. The Zn-foil was irradiated at a thermal neutron flux of $4.24 \cdot 10^{17}$ $m^{-2}s^{-1}$ for 6 h, and subsequently, dissolved in 8 M nitric acid (HNO_3), slowly dried down on a heating plate, and redissolved in Milli-Q water. Y_2O_3, and La_2O_3 were irradiated at a thermal neutron flux of $4.69 \cdot 10^{16}$ $m^{-2}s^{-1}$ for 3 h and subsequently, dissolved in 1 M HNO_3 solution, slowly dried down on a heating plate, and redissolved in Milli-Q water. The radiotracer Ga-68 was eluted from an Eckert & Ziegler IGG100 GMP Ge-68/Ga-68 generator (generously supplied by Erasmus MC, the Netherlands) in 0.1 M HCl. The radiotracer Ac-225 was supplied by Eckert & Ziegler and Ra-223 was supplied by GE Healthcare.

Radioactivity measurements of the radiotracers were performed as follows: The Wallac Wizard2 3" 2480 Automatic Gamma Counter from Perkin Elmer (Groningen, the Netherlands) was used for gamma-radiation measurements of La-140, Cu-64, Ga-68, and Ra-223, while the beta-emitting Y-90 was measured with a Liquid Scintillation Counter (tri-carb 2750TR/LL, Packard). Ac-225 was measured indirectly at equilibrium (> 30 minutes after experiments) with its γ-emitting daughter Fr-221 ($t_{1/2} = 4.9$ minutes).

2.5. Separation of radionuclides with chelator-impregnated PDMS beads

2.5.1. Sorption capacity

To measure the sorption capacity of chelator-impregnated PDMS beads for different radionuclide-chelator combinations, 10 mg of the impregnated beads was submerged in 1 mL aqueous solutions with known concentration of Y (1 μM), La (1 μM), Cu (1 nM), or Ga (1 nM). The corresponding radioactive tracers Y-90, La-140, Cu-64, and Ga-68 were added to their respective solutions at concentrations between 1–10 kBq/mL. For Y and La, PDMS beads impregnated with the chelator D2EHPA were selected. For Cu and Ga, DTZ and BPHA were chosen, respectively, due to their use in prior studies on microfluidic solvent extraction of Cu-64 [26,27] and Ga-68 [28]. The solutions containing Y and La had a pH of 6, the Cu solution had a pH of 0, and the Ga solution had a pH of 2, according to the optimal pH for the extraction with these chelators, as determined by solvent extraction experiments [26–28]. The vials containing the aqueous solutions and PDMS beads were put on a Vortex-Genie 2 (Scientific Industries, Inc) at the highest speed for 1 h to ensure equilibrium was reached. Afterwards, the aqueous

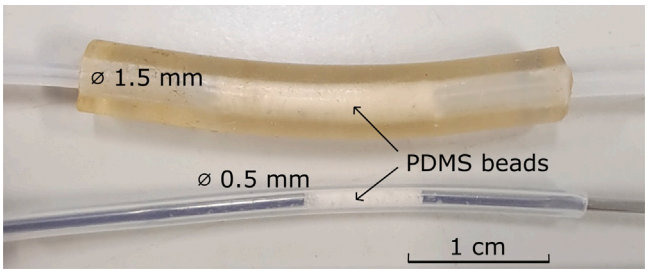

Fig. 2. Chromatography columns with chelator-impregnated PDMS beads used for the separation of radionuclides from their target. D2EHPA-impregnated PDMS beads in a column with an inner diameter of 1.5 mm used for the in-flow separation of Y and La (top; loading 20 mg) and in a column with an inner diameter of 0.5 mm used for the in-flow separation of Ac-225 (bottom; loading 5 mg).

solutions were pipetted out of the vials, avoiding the PDMS beads. The concentration of Y, La, Cu, and Ga in the aqueous solutions was determined by measuring the radioactivity A of their corresponding radiotracers, which are representative of the total concentrations. The sorption capacity was calculated by subtracting the measured amount of Y-90, La-140, Cu-64, or Ga-68 after the adsorption ($n_{\text{aq, depleted}}$) from the initial amount ($n_{\text{aq, initial}}$), and dividing the adsorbed amount by the mass of the chelator-impregnated PDMS beads (m_{beads}), i.e.,

$$Sorption\ capacity\ [\frac{\text{mol}}{\text{g}}] = \frac{n_{\text{aq, initial}}\ [\text{mol}] - n_{\text{aq, depleted}}\ [\text{mol}]}{m_{\text{beads}}\ [\text{g}]}. \quad (1)$$

Experiments were done in triplicate and errors are given as one standard deviation of the mean.

2.5.2. In-flow separation

To test the in-flow separation of Y from Sr and La from Ba, 20 mg of D2EHPA-impregnated PDMS beads were loaded into a tubing with a diameter of 1.5 mm (Fig. 2, top). The solutions consisted of 1 M $Sr(NO_3)_2$ with 100 μM $[^{90}Y]Y(NO_3)_2$ or 0.1 M $Ba(NO_3)_2$ with 10 μM $[^{140}La]La(NO_3)_2$, dissolved in Milli-Q water (nomenclature adapted from [52]). For the Ac-225 separation from $[^{223}Ra]Ba(NO_3)_2$, only 5 mg of D2EHPA-impregnated PDMS beads were loaded into a tubing with a diameter of 0.5 mm (Fig. 2, bottom), because of the significantly lower Ac-225 concentration in the solution (in the picomolar range, compared to the micromolar range for Y and La). The solution consisted of 0.1 M $Ba(NO_3)_2$ with ~ 10 kBq/mL Ac-225 and ~ 10 kBq/mL of Ra-223. These model solutions were used for the experiments to collect results, upon which future experiments with irradiated targets can be designed. The aqueous solutions containing the radionuclides were filled into syringes and pushed through the column by a syringe pump (AL-1000 Programmable Syringe pump 941-371-1003 from World Precision Instruments Inc.) at various flow rates in the range of 0.1–6 mL/min. The adsorption efficiency (AE) was defined as the relative difference in measured radioactivity before (A_{initial}) and after ($A_{\text{after adsorption}}$) the in-flow separation, i.e.,

$$AE\ [\%] = \left(1 - \frac{A_{\text{after adsorption}}}{A_{\text{initial}}}\right) \times 100\%. \quad (2)$$

After the adsorption, the radionuclide of interest needs to be eluted from the beads into another aqueous solution. Herefore, different HCl concentrations were tested, ranging from 0.1 M to 4 M HCl, to see if a difference in acidity leads to a difference in elution speed. The flow rate was kept at 0.1 mL/min. 100 μL fractions were collected consecutively and their radioactivity was measured as described above.

Co-adsorption of Sr, Ba, and Ra-223, from 1 M $Sr(NO_3)_2$ for Sr, and 0.1 M $Ba(NO_3)_2$ for Ba and Ra-223, was also studied in-flow using the above procedure and the adsorption efficiency was determined according to Eq. (2). Of note, for Sr and Ba, instead of the ratio of the radioactivities, we used the ratio of the concentrations before and after the in-flow separation as measured by inductively coupled plasma mass spectrometry (ICP-MS, Perkin Elmer, NexION 2000).

For the separation of Ac-225 from Ra-223 a separation factor (S) was calculated additionally, for the results at the optimal flowrate of 0.3 mL/min, according to Eq. (3), where D is defined as the ratio of the adsorbed and not adsorbed radioactivity.

$$S = \frac{D_{\text{Ac}}}{D_{\text{Ra}}} \quad (3)$$

The co-adsorption of the potential metal contaminants Ni, Fe, Cu, Zn, Pb, Al, and Ca to the D2EHPA-impregnated PDMS beads was studied as well. These contaminations are commonly found in irradiated targets [53]. They are essential to study, since one important parameter for the use of the already separated radionuclides is the specific activity, which is the radioactivity per unit mass. A solution consisting of 100 μg/L of each metal contaminant was flown through the column as described above. We used a flow rate of 0.3 mL/min, which was identified as the optimal flow rate for Ac-225 adsorption as explained later. The initial concentrations and concentrations after the adsorption, as well as the elution into 0.1 M HCl (in which Ac-225 is collected), were measured by ICP-MS and the AE was calculated as described above. The total recovery of the contaminants was calculated as

$$Total\ recovery\ [\%] = \frac{c_{\text{elution}}}{c_{\text{initial}}} \times 100\%, \quad (4)$$

where c_{elution} is the measured concentration of the contaminant in the elution and c_{initial} is the initial concentration of the contaminant in the solution during the in-flow separation. All experiments were executed in triplicate and errors are given as one standard deviation of the mean.

3. Result and discussion

3.1. PDMS beads impregnated with three different chelators

Fig. 3 shows the FTIR spectra of bare PDMS beads and PDMS beads impregnated with three different chelators. These spectra confirm the presence of the chelators on the impregnated beads, evident from peaks in the spectra specific to the specific bonds in the molecular structure of the different chelators. For BPHA, its presence is confirmed by the peak on the wavelength of 1622 cm^{-1} associated with the C=O bond of BPHA and on the wavelength of 3171 cm^{-1} associated with the O-H bond [50], see Fig. 3(a). For D2EHPA, its presence is confirmed by the peak on 1230 cm^{-1} corresponding to the P=O bond of D2EHPA and by extra stretching in the 3000–2900 cm^{-1} region, see Fig. 3(b). Although DTZ is harder to observe than the other two chelators as most of its characteristic peaks overlap with the peaks of PDMS, we confirm the presence of DTZ by the peaks in the 3000–2900 cm^{-1} region, see Fig. 3(c).

Since the final application of the chelator-impregnated PDMS beads is to adsorb radionuclides, the chelators are preferably located at the outer surface, where most of the adsorption takes place. While FTIR spectra indicate the presence of the characteristic peaks corresponding to the chemical groups of the chelators, its penetration depth is relatively high (in μm range), and it does not reveal where the chelators are present. Therefore, we approached this hypothesis with additional FE-SEM and XPS measurements. The FE-SEM images show that the surface morphology changes with the impregnation, see Figure A.2. More specifically, particle-like structures are seen on the surface of the PDMS beads impregnated with BPHA and DTZ, while a smoothening-like effect is observed on the surface of the PDMS beads impregnated with D2EHPA. This difference may arise from the fact that D2EHPA is in liquid form at room temperature, while DPHA and DTZ are in powder form when dissolved in chloroform. Furthermore, the XPS survey spectra show the presence of characteristic atomic peaks on the first few nanometers of the surface of the samples: a nitrogen peak on the PDMS impregnated with BPHA, a phosphorus peak on the PDMS

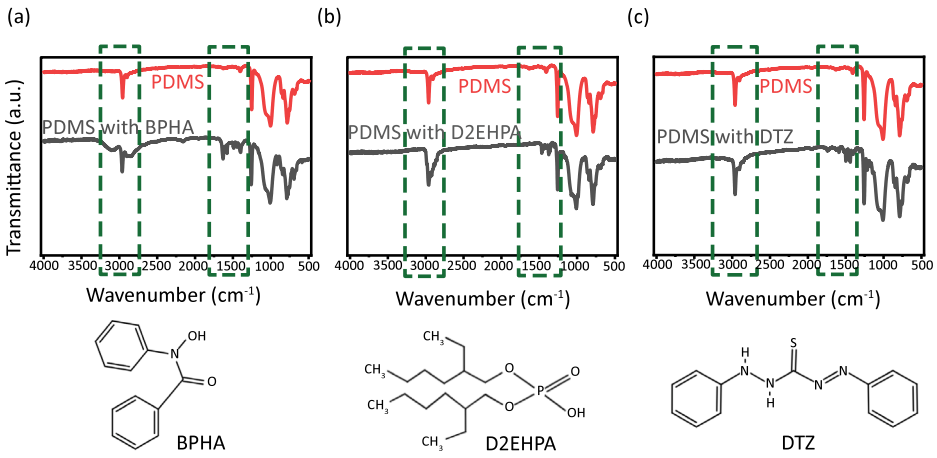

Fig. 3. Presence of the chelators on the impregnated PDMS beads by FTIR. FTIR spectra of bare PDMS beads and PDMS beads impregnated with the chelators BPHA (a), D2EHPA (b), and DTZ (c), along with their corresponding chemical structure. The spectra of bare PDMS beads are in red, the spectra of the impregnated PDMS beads are in grey, and the peaks characteristic for the chelators are highlighted in the green boxes. The FTIR of the pure chelators can be found in literature [35,50,54].

impregnated with D2EHPA, and a nitrogen peak, and a sulfur peak on the PDMS impregnated with DTZ, see Figure A.3. The XPS survey scans on the surface thus agree with the visual FE-SEM inspections, which indicates that the chelators may be present on the surface of the PDMS beads. Interestingly, the depth profiling of the samples shows the characteristics peaks even after etching of 400 seconds, see Figure A.3. This indicates infiltration of the chelators inside the PDMS beads. This infiltration is explained by the entrapment of the chelators in the matrix of PDMS during the chloroform swelling process [55]. This swelling process hence is important, increasing the loading capacity of the chelators in the PDMS beads.

To investigate further whether the chelators are chemically or physically sorbed, the XPS survey scans of Si2p are resolved. The Si2p peaks are chosen as they are exclusive peaks present in PDMS beads and not in the chelators. Figure A.4 shows the scan of Si2p where both bare PDMS and PDMS impregnated with three different chelators have comparable peaks, indicating no chemical changes in the Si atomic bond. This result implies the absence of a chemical interaction between the chelators and the Si atoms of the PDMS beads. Additionally, we conducted and resolved XPS survey scans of C1S. From Figure A.4, there are extra peaks visible in the C1s scans (at 288.1 eV) of the chelators-impregnated PDMS beads when compared with the C1s scans of bare PDMS beads. These peaks correspond to the presence of C–O bonds in the samples. However, this C–O bond is typically present in BPHA, D2EHPA, and DTZ. Thus, to infer the presence of chemical interaction between PDMS beads and the chelators from this bond is difficult. Furthermore, most C1s peaks (as well as the O1s peaks) also experience broadening and shifts, common occurrences in non-conductive samples such as PDMS beads. The broadening and the shifts of the peaks make the inferring of the resolve less reliable. From the resolves of Si2p, we hence argue that the impregnation process, as indicated by other works [20,56], is a physisorption process, with a swelling-induced transport of chelators into the matrix of the PDMS beads.

Since the maximum sorption capacity is limited by the amount of chelators present, it is important to quantify the amount of impregnated chelators on the PDMS beads. We determined this amount based on thermogravimetry. We measured the mass of the beads at temperatures increasing from 25 °C to 800 °C and calculated the mass of the samples impregnated with the three types of chelators at various concentrations relative to the initial mass of the samples at 100 °C. Following the common practice of assuming that the mass decline between 25 °C and 100 °C is due to sample dehydration, we consider the mass difference between bare PDMS beads and impregnated PDMS beads at 310 °C, where bare PDMS starts decreasing in mass, as an approximation of the total mass of the impregnated chelators. For BPHA-impregnated PDMS beads, the mass difference increases from 1.8% ±0.1% for PDMS beads impregnated with 0.10 M BPHA in chloroform to 3.7% ±0.1% and 9.7% ± 0.2% for PDMS beads impregnated with 0.25 M and 0.75 M BPHA in chloroform, respectively, see Fig. 4(a). This indicates an increasing BPHA amount impregnated in the PDMS beads as the available BPHA in chloroform increases. Since the solubility of BPHA in chloroform is around 155 g L^{-1} (equivalent to 0.72 M [33]), we suspect that the impregnated BPHA amount does not increase further. This hypothesis is supported by the TGA results of DTZ-impregnated PDMS beads where the beads impregnated with 0.01 M DTZ in chloroform show a mass difference of 1.4% ± 0.1%, while the beads impregnated with DTZ solutions of 0.10 M and 0.25 M, above their saturation concentration (solubility of DTZ is 17 g L^{-1} or 0.075 M in chloroform [34]) show no significant difference in their mass difference (7.4% ± 1.0%, and 8.9% ± 1.7%, respectively), see Fig. 4(c). For D2EHPA, liquid at room temperature, a similar trend of increasing mass difference between PDMS beads impregnated with 0.10 M and 0.25 M D2EHPA in chloroform is observed, from 21.0% ± 0.9% to 30.9% ± 1.1%, see Fig. 4(b). The difference does not significantly increase when the beads are impregnated with 0.75 M (31.3% ± 1.2%), indicating the maximum capacity of the PDMS matrix in accommodating D2EHPA. To confirm this hypothesis about PDMS matrix capacity, we conduct an additional swelling test. We immerse bare PDMS bead samples in chloroform for 10 h and measure a volumetric increase of 16.0% ± 2.2% and a mass increase of 23.4% ± 3.1%. This PDMS volumetric increase due to swelling corresponds well with the mass increase, as the density of chloroform is 1.489 g mL^{-1}, indicating the filling of the PDMS matrix with chloroform. However, when we apply a similar calculation to 0.25 M D2EHPA-impregnated PDMS beads samples, the expected mass increase (15.6%, the density of D2EHPA is 0.976 g mL^{-1}) due to D2EHPA impregnation is lower than the measured mass decrease by TGA (30.9% ± 1.1%). This difference could happen due to the adsorption of D2EHPA on the surface of the PDMS beads. To resolve this, we reduce the surface adsorption effect by immersing a PDMS block with a lower surface-to-volume ratio (1 cm × 1 cm × 1 cm) in a similar chloroform solution containing 0.25 M D2EHPA. We then conduct TGA measurements on the cut samples to approximate the amount of the impregnated D2EHPA. The result shows a much lower mass decrease (15.8%) compared to the bead samples. This measured mass decrease is closer to the calculated mass increase due to swelling. From both tests, we argue that the total impregnated chelator amount is the sum of the amount of D2EHPA accommodated inside the PDMS matrix and the amount of D2EHPA located on the surface. This result also emphasizes the importance of the PDMS beads' diameter, where a smaller diameter

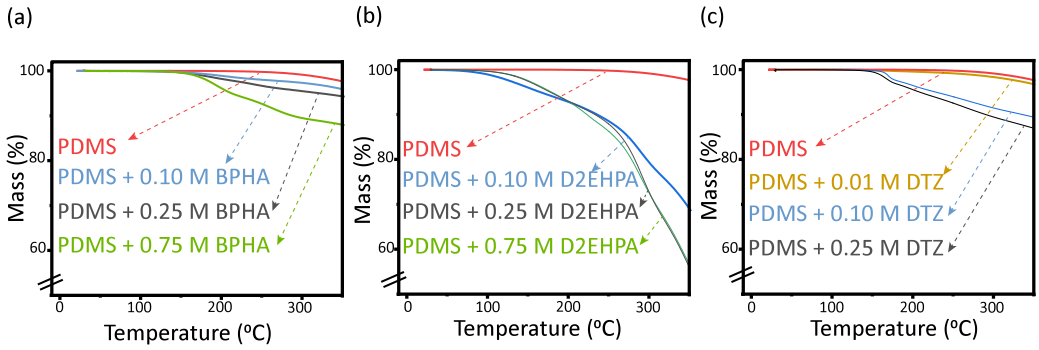

Fig. 4. Quantification of the amount of chelator impregnated in the PDMS beads using thermogravimetry. Thermogravimetry of PDMS beads impregnated with BPHA (a), D2EHPA (b), and DTZ (c) at various concentrations of these chelators in chloroform.

leads to an increase in surface area and subsequently an increase in the impregnation amount. While this study focuses on a fabrication method using simple kitchen equipment, there have been many studies on increasing the surface area of PDMS beads (e.g., PDMS beads with a median diameter of 1 μm obtained using droplet microfluidics [57] or porous PDMS using template moulding [58]). We note that Fig. 4 also implies that the chelator-impregnated PDMS beads are stable at temperatures below 120 °C.

3.2. Chemical stability of the chelator-impregnated PDMS beads

A known problem in the applications of chelator-impregnated resins is the low chemical stability, leading to leaching of the impregnated chelator over time, causing contamination during elution [21,25]. To assess the chemical stability of the chelator-impregnated PDMS beads, we immerse the beads in three solutions of different acidity: Milli-Q water, 1 M HCl, and 12 M HCl. For D2EHPA-impregnated PDMS beads, the XPS spectra obtained after washing and drying are shown in Fig. 5(a). P2p peaks are observed in all samples, indicating the presence of D2EHPA in all the samples. Furthermore, the phosphorus atom remains in a phosphate form (at 134 eV) with no significant chemical state change even after washing it with 12 M HCl. The Cl2p spectra show no chlorine sorbed into the PDMS beads, reducing the possibility of contamination during the separation of the radionuclides. Complementing the XPS results, Fig. 5(b) shows the UV–Vis spectra of the immersion solutions. Pure D2EHPA (100%(v/v)) shows a peak at 274 nm [59], while no peaks are observed in all liquid samples after 5 minutes of immersion, indicating at least no detectable D2EHPA. The liquids remain visibly clear and no fluid separation after 24 h is observed. On the other hand, the immersing liquid from D2EHPA-impregnated silica powder is opaque and cloudy, indicating the presence of dispersed D2EHPA. After decanting, these impregnated silica samples show a D2EHPA release of 220 mg/g ± 13 mg/g, 45 mg/g ± 11 mg/g, and 52 mg/g ± 12 mg/g in Milli-Q water, 1 M HCl, and 12 M HCl, respectively. When we challenge the stability of the D2EHPA-impregnated PDMS beads by immersing them in both 1 M HCl and 12 M HCl for a longer period (8 h), as well as in a different acid (1 M HNO_3), we find no indication of leached D2EHPA aside from the samples immersed for 8 h in 12 M HCl, see Fig. 5(b).

To compare with the D2EHPA-impregnated PDMS beads, we carry out the stability tests for BPHA-impregnated PDMS beads and DTZ-impregnated PDMS beads along with BPHA- and DTZ-impregnated silica powder. As expected, all BPHA-impregnated PDMS samples (washed and non-washed) show the presence of N1s peaks in the XPS spectra, while no BPHA-indicative peaks are found in the immersing liquids around 200 nm (indicating the N-phenylhydroxamide group [60]) in the UV–Vis spectra, see Figure A.5(a) and (c), respectively. Please note that the shape of the N1s peaks in the XPS spectra of non-washed BPHA-impregnated PDMS samples is different from those washed due to protonation of BPHA, as reported in previous work [61]. Similar behaviour is observed for all DTZ-impregnated PDMS samples, with the presence of N1s XPS peaks for washed and non-washed beads, while no peaks are found in the immersing liquids around 450 nm and 618 nm (indicative for DTZ [62]), see Figure A.5(b) and (d), respectively. In contrast, all immersion liquids of the impregnated silica powder samples show intense peaks in the UV–Vis spectra, see Figure A.5(e) and (f). Please note that in Figure A.5(f), the peaks shifted due to possible oxidization of DTZ [62].

To understand the reason behind the stability of the impregnated chelator on PDMS beads, we evaluated the interactions between the chelator and PDMS in an aqueous medium using the extended Derjaguin–Landau–Verwey–Overbeek (EDLVO) theory [47,63]. We determined the Gibbs free energy using this theory, complemented by a series of contact angle measurements. The Gibbs free energy indicates the presence (or absence) of hydrophobic interactions, a common interaction found in polymeric materials, where a negative Gibbs free energy indicates the presence of hydrophobic interactions [46,48,64]. Fig. 6(a) shows the measured contact angle of three different liquids on PDMS and the three different chelators. Additionally, reference measurements were performed on silica. Our reported contact angle values for PDMS and silica are comparable with previous works [65–68]. Fig. 6(b) shows the subsequently calculated Gibbs free energy. The interaction between PDMS and all three chelators shows a negative Gibbs free energy, indicating the presence of hydrophobic interaction. This is consistent with previous works on PDMS [69–71]. From Fig. 6(b), most of the negative Gibbs free energy for the PDMS-chelator combinations is contributed by the acid–base interaction (ranging from −20 kT to −60 kT), while the Lifshiftz-van der Waals interaction contributes much less (~−1 kT). This suggests that the resulting hydrophobic interaction is due to hydration repulsion towards the chelators instead of a direct attraction force of PDMS [72,73]. Furthermore, while the interaction between PDMS and D2EHPA, and PDMS and DTZ show comparable negative values, the interaction between PDMS and BPHA shows a less negative Gibbs free energy, implying a relatively weaker hydrophobic interaction. This result is in line with the theoretical use of the octanol-water partition coefficient (K_{ow}) of the chelators to predict the sorption behaviour (and sorption strength) of the chelators [74] on hydrophobic material. A positive K_{ow} indicates a partition preference of the chelators in octanol (as opposed to water), with higher K_{ow} indicating a higher octanol partition, and subsequently stronger hydrophobic interaction. Previous works indicate K_{ow} of 4 for D2EHPA [75]; 3-4 for DTZ [76] and 2-3 for BPHA [77].

In sharp contrast to the interaction between the chelators and PDMS, we find that all interactions between the chelators and silica show a positive Gibbs free energy, explaining the high release of the chelators when immersed in an aqueous medium (Figure A.5). Please note that this approach neglects a plausible complementary phenomenon where the chelator molecules are physically trapped in

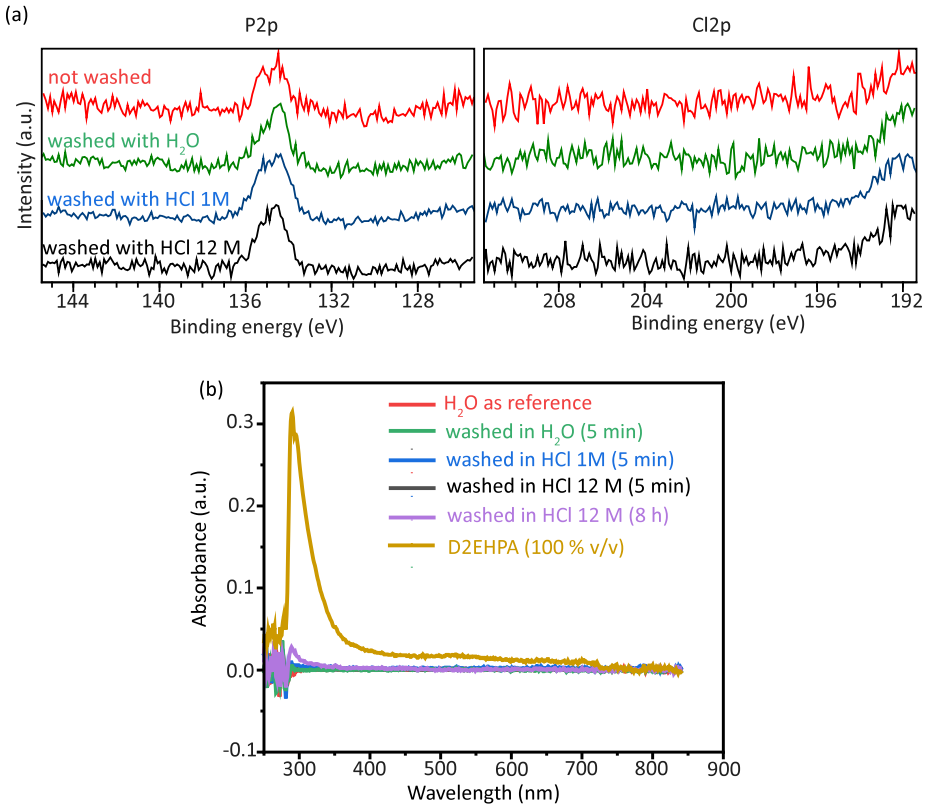

Fig. 5. Chemical stability of D2EHPA-impregnated PDMS beads against leaching measured with XPS and UV–Vis. (a) XPS P2p scan and Cl2p scan of D2EHPA-impregnated PDMS beads before and after 5 minutes of immersion in solutions of different acidity (b) the corresponding UV–Vis spectra of the immersion solutions.

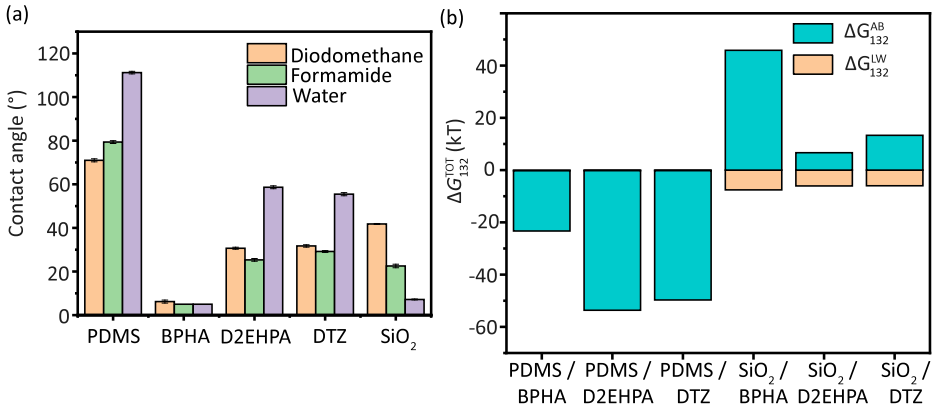

Fig. 6. Approximation of hydrophobic interaction between PDMS beads and chelators. (a) The average measured static contact angle of non-polar liquid diiodomethane and polar liquid formamide and water on various substrates (the error bars represent 1 standard deviation from the average) and (b) Gibbs free energy calculated for estimating the interaction strength using the extended Derjaguin–Landau–Verwey–Overbeek approach.

the PDMS matrix and therefore become immobile. While this complimentary effect is not incorporated, the comparison to the silica samples already shows that chelators are more strongly bound to PDMS beads than to silica powders.

3.3. Sorption capacity of PDMS beads with different chelators

Table 1 shows the measured sorption capacity of D2EHPA-, DTZ-, and BPHA-impregnated PDMS beads, for Y, La, Cu, and Ga, respectively. The results show a much higher sorption capacity of the D2EHPA-impregnated PDMS beads over the DTZ- and BPHA-impregnated PDMS beads. More specifically, the D2EHPA-impregnated PDMS beads have a six orders of magnitude higher sorption capacity towards Y and La than the DTZ-impregnated PDMS beads have towards Cu, and a seven orders of magnitude higher sorption capacity than the BPHA-impregnated PDMS beads have towards Ga. This proves again the significantly higher integration of D2EHPA into the PDMS compared to

Table 1
Sorption capacity. Sorption capacity of PDMS beads with different chelators, specific for Yttrium (Y), Lanthanum (La), Copper (Cu), and Gallium (Ga) ($n = 3$).

Chelator	Element	Sorption capacity
D2EHPA	Y	2.75 ± 0.53 mg/g
D2EHPA	La	4.03 ± 0.41 mg/g
DTZ	Cu	4.0 ± 1.1 ng/g
BPHA	Ga	0.329 ± 0.092 ng/g

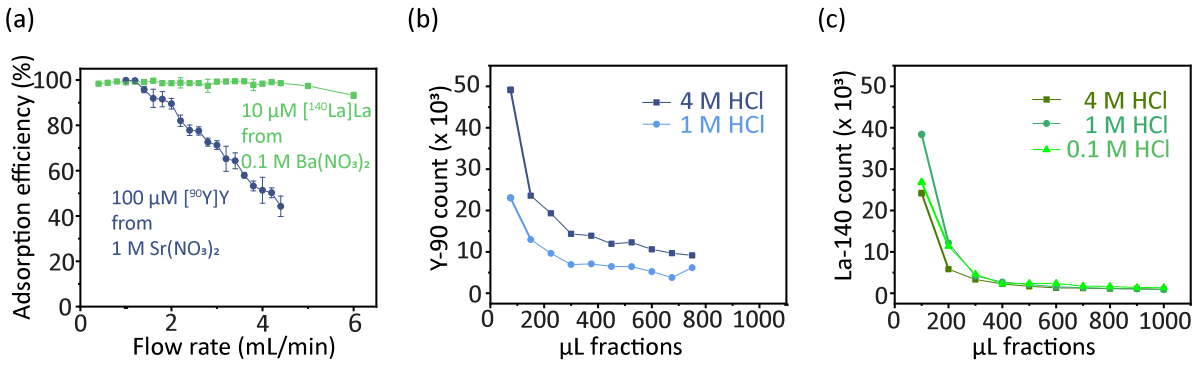

Fig. 7. Chromatography column separation and elution with D2EHPA-impregnated PDMS beads for Y and La. (a) In-flow separation of 10 µM [^{140}La]La and 100 µM [^{90}Y]Y from their respective target solutions of 0.1 M $Ba(NO_3)_2$ and 1 M $Sr(NO_3)_2$ ($n = 3$). (b) Elution profile of [^{90}Y]Y into 4 M and 1 M HCl at a flow rate of 0.1 mL/min ($n = 1$). (c) Elution profile of [^{140}La]La into 4 M, 1 M and 0.1 M HCl at a flow rate of 0.1 mL/min ($n = 1$).

BPHA and DTZ, with the underlying reasons discussed in the previous section.

In comparison to other commercial ion-exchange resins, the D2EHPA-impregnated beads show a lower sorption capacity. For example, the Dowex 50W-X8 resin has a sorption capacity towards rare earth elements between 191 and 294 mg/g [78], Ln resin has a sorption capacity of 30.67 mg/g for Eu [79], the Amberlite IR120H (AIR120H) resin has a sorption capacity of 8.2 mg/g for Ce [80], and HDEHP-loaded microcapsules (impregnated) have a sorption capacity of 58.07 mg/g for Eu [79]. While the primary focus of this work is on the development of a selective and stable resin, we note that optimizing the sorption capacity for the chelator-impregnated beads is outside the scope of the present work. We expect that higher sorption capacities can be obtained, for example by optimization of the diameter and the porosity of the beads for example as shown by [81] and [57]).

3.4. In-flow separation with D2EHPA-impregnated PDMS beads

Given the high chemical stability and the higher sorption capacities of the D2EHPA-impregnated PDMS beads for Y and La, we continued with in-flow separation and elution studies using a chromatography column with these combinations of chelator and radionuclides. For the separation of La from its Ba target, we prepared an aqueous 10 µM La (and a La-140 radiotracer with 0.1 M $Ba(NO_3)_2$) solution and injected the mixture at various flow rates in the column to study the influence of the residence time on the adsorption efficiency. For the separation of Y from its Sr target, an aqueous solution containing 100 µM Y (and a Y-90 radiotracer) and 1 M $Sr(NO_3)_2$ was prepared, and injected in the column.

For the lowest range of flow rates studied, we observe that both Y and La are adsorbed to the D2EHPA-impregnated PDMS beads with almost 100% adsorption efficiency, see Fig. 7(a). For increasing flow rates, i.e., decreasing residence times, the adsorption efficiency declines. A notable decline is observed for flow rates above 1 mL/min and 4.5 mL/min for Y and La, respectively. Apart from this difference in onset, we also observe a clear difference in slope. While the adsorption efficiency already decreases from 99.89% ± 0.14% at 1 mL/min to 77.5% ± 1.8% at 2.6 mL/min for Y, it only decreases from 99.50% ± 0.12% at 4.5 mL/min to 91.1% ± 1.4% at 6 mL/min for La. The difference in onset and slope might be explained by (I) the concentration of Y being ten times higher than the concentration of La in their respective solutions and (II) the smaller ionic radius of Y.

For the application of the chelator-impregnated PDMS beads in the field of nuclear medicine, it is not only important that the adsorption efficiency of the radionuclide of interest is close to 100%, but also that the adsorption efficiency of the corresponding target is as low as possible. We therefore also measured the co-adsorption of the Ba and Sr target solutions at the largest flow rates that still result in high adsorption efficiencies of La and Y. Ba co-adsorption was measured to be 1.28% ± 0.45% at a flow rate of 4 mL/min and Sr co-adsorption was 1.24% ± 0.57% at a flow rate of 1 mL/min. From these results, the co-adsorption of the corresponding target material is low, showing a promising application in the clinical field.

Elution of Y and La from the D2EHPA-impregnated PDMS beads was studied for elution solutions of different acidity. We observe that elution of Y is incomplete after 1 mL and only around 65%, while the elution of La is about 85% in the first 1 mL, see Fig. 7(b) and (c). The difference in behaviour might be due to the higher concentration of Y, necessitating higher volumes to increase the total elution. The acidity of the solutions does not significantly influence the elution profiles. Additionally, the smaller ionic size of Y leads to a more stable complex with D2EHPA. This trend of increasing complex stability with increasing charge density (i.e., decreasing ionic radius) is often found in chelate complexation [82] and was shown before for lanthanide and actinide complexes [83], making it more difficult to fully elute in small volumes.

A radionuclide that currently receives increasing attention for its potential in targeted alpha therapy is Ac-225. For this reason, we also studied the in-flow separation Ac-225 from its target Ra-223 and its subsequent elution in a chromatography column loaded with D2EHPA-impregnated PDMS beads. Since the total concentration of Ac-225 compared to Y and La was significantly lower by nine orders of magnitude, only 5 mg of PDMS beads was used. The results again show an adsorption efficiency close to 100% for the lower range of flow rates, with a decline in adsorption efficiency for increasing flow rate, see Fig. 8(a). At a flow rate of 0.3 mL/min, the adsorption efficiency of Ac-225 is 98.51% ± 0.25%, while the co-adsorption of its target Ra-223 is 0.94% ± 0.57%.

Elution of Ac-225 was achieved with 0.1 M HCl at a flow rate of 0.1 mL/min. 80.3% ± 0.9% of Ac-225 was eluted in the first 1 mL and 93.2% ± 1.7% in the first 2 mL, see Fig. 8(b). The final eluted solution contains 0.053% ± 0.014% of the initial amount of Ra-223 in the first 1 mL and a total of 0.068% ± 0.015% in 2 mL, resulting in a separation factor that averages over 6000. We note that we washed the column before the elution of Ac-225 with the 0.1 M HCl solution with Milli-Q water, which reduced the amount of Ra-223 in the elution solution by 90.8% ± 2.5%.

A known problem that may arise during the production of Ac-225 is the contamination of the Ac-225 solution with metal contaminants during production as reported by Ramogida et al. [53]. For this reason, we studied the in-flow separation and elution of metals as well. Table 2 shows the adsorption efficiency and the total recovery. From all measured metal contaminants only Zn is co-adsorbed at 15.7% ± 7.1% and also fully eluted in 0.1 M HCl, resulting in a total recovery of 15.1% ± 7.1% in the elution fraction. While Fe shows a high AE of 82.8% ± 4.6%, it is not eluted in 0.1 M HCl and only 1.38% ± 0.24% of the

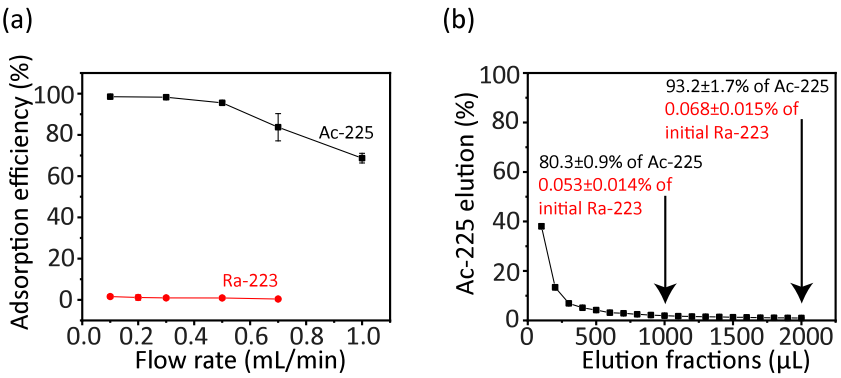

Fig. 8. Chromatography column separation and elution with D2EHPA-impregnated PDMS beads for Ac-225. (a) In-flow separation of Ac-225 at different flow rates ($n = 3$). (b) Elution profile of Ac-225 indicated by Fr-221 in 0.1 M HCl at a flow rate of 0.1 mL/min ($n = 2$).

Table 2
Adsorption of metal contaminants during the separation of Ac-225. Adsorption efficiency (AE) and total recovery of the metal contaminants in the 0.1 M HCl elution. The concentrations of the metals were 100 µg/L. Experiments were done in triplicate and errors are given as one standard deviation of the mean.

	Ni	Fe	Cu	Zn	Pb	Al	Ca
AE [%]	0.99 ± 0.86	82.8 ± 4.6	0.95 ± 0.64	15.7 ± 7.1	14.5 ± 6.6	48.1 ± 1.8	11.78 ± 0.88
Recovery [%]	0.020 ± 0.003	1.38 ± 0.24	0.92 ± 0.06	15.1 ± 7.1	4.8 ± 1.5	0.13 ± 0.08	3.81 ± 0.97

initial amount is present in the elution solution, meaning that it is also cleared from the target solution. All other tested elements are neither co-adsorbed nor eluted in significant amounts. These results indicate a high decontamination during the Ac-225 separation with the presented D2EHPA-impregnated PDMS beads.

Overall, the D2EHPA-impregnated PDMS beads have proved successful in the separation of Ac-225 from [^{223}Ra]Ba(NO_3)$_2$ with around 93% of Ac-225 and below 0.1% of Ra-223 in the first 2 mL of elution. In comparison, multiple other methods have been investigated in the literature for the separation of Ac-225 from radium targets, including ion-exchange column chromatography (using AG50 × 8 [84] or AG50X4 [85], Ln- [86] or DGA resin [87]), microfluidic ion-exchange [85], as well as solvent impregnated resins [88]. While all of these methods achieve a good separation of Ac-225, they all show different drawbacks, such as the need for (i) large volumes of chemicals [84,87,88], (ii) highly acidic solutions for elution [84,85,88], (iii) slow processing [85,88], or (iv) additional clean-up steps [86]. Furthermore, it has been reported that DGA resin is highly sensitive to radiolysis and extra washing steps are needed to reduce radiolytic degradation products [87], partially due to the characteristic water loading [89]. While it remains to be shown if the presented D2EHPA-impregnated PDMS beads have a higher radiation stability, D2EHPA and PDMS separately are reportedly highly resistant against radiation [90,91]. Thus, in comparison with existing separation methods, the presented chelator-impregnated PDMS beads are promising to separate medical radionuclides in a commercial setting.

4. Conclusions

We presented chelator-impregnated PDMS beads that allow the selective and efficient separation of the medically-interesting radionuclides (Y-90, La-140, and Ac-225) from their liquid target ($Sr(NO_3)_2$, $Ba(NO_3)_2$, and [^{223}Ra]Ba(NO_3)$_2$), with minimal leaching of the chelator from the beads when contacted with the acidic solutions used for adsorption and subsequent elution of the radionuclides. This minimal leaching is beneficial for the purity of the radionuclide solution and at the same time offers the possibility of direct liquid target recycling. The simple fabrication of the chelator-impregnated PDMS beads together with the ability to impregnate PDMS with different types of chelators offers a versatile approach towards increasing the applicability of chelators for the simple, automatable separation of medical radionuclides.

CRediT authorship contribution statement

Albert Santoso: Conceptualization, Methodology, Validation, Formal analysis, Investigation, Data curation, Writing – original draft, Visualization. **Svenja Trapp:** Conceptualization, Methodology, Validation, Formal analysis, Investigation, Data curation, Writing – original draft, Visualization. **Iris M.S. Blommestein:** Methodology, Validation, Formal analysis, Investigation, Data curation, Writing – review & editing. **Saeed Saedy:** Methodology, Validation, Formal analysis, Investigation, Data curation, Writing – review & editing. **J. Ruud van Ommen:** Conceptualization, Project administration, Writing – review & editing, Supervision. **Robin M. de Kruijff:** Conceptualization, Project administration, Writing – review & editing, Supervision. **Volkert van Steijn:** Conceptualization, Project administration, Writing –review & editing, Supervision.

Declaration of competing interest

The authors declare that they have no known competing financial interests or personal relationships that could have appeared to influence the work reported in this paper.

Data availability

Data will be made available on request.

Acknowledgements

This publication is part of the Open Technology Programme (with project number 16913) financed by the Dutch Research Council (NWO). We would like to acknowledge Baukje Terpstra and Astrid van der Meer for their assistance with the irradiations at the HOR. We extend our gratitude to Bart van der Linden and Willie Rook for the technical support with TGA, to Bart Boshuizen for the fruitful discussion on the XPS results, and to Bijoy Bera for the fruitful discussion on the surface energy. We acknowledge the use of BioRender.com to partially make the figures.

Appendix A. Supplementary data

Supplementary material related to this article can be found online at https://doi.org/10.1016/j.seppur.2024.128865.

References

[1] W. Oyen, L. Bodei, F. Giammarile, H. Maecke, J. Tennvall, M. Luster, B. Brans, Targeted therapy in nuclear medicine—current status and future prospects, Ann. Oncol. 18 (2007) 1782–1792, http://dx.doi.org/10.1093/annonc/mdm111.

[2] W.A. Weber, J. Czernin, C.J. Anderson, R.D. Badawi, H. Barthel, F. Bengel, L. Bodei, I. Buvat, M. DiCarli, M.M. Graham, J. Grimm, K. Herrmann, L. Kostakoglu, J.S. Lewis, D.A. Mankoff, T.E. Peterson, H. Schelbert, H. Schöder, B.A. Siegel, H.W. Strauss, The future of nuclear medicine, molecular imaging, and theranostics, J. Nucl. Med. 61 (2020) 263S–272S, http://dx.doi.org/10.2967/jnumed.120.254532.

[3] A. Sanchez-Crespo, Comparison of gallium-68 and fluorine-18 imaging characteristics in positron emission tomography, Appl. Radiat. Isot. 76 (2013) 55–62, http://dx.doi.org/10.1016/j.apradiso.2012.06.034.

[4] G. Crişan, N.S. Moldovean-Cioroianu, D.-G. Timaru, G. Andrieş, C. Căinap, V. Chiş, Radiopharmaceuticals for PET and SPECT imaging: A literature review over the last decade, Int. J. Mol. Sci. 23 (2022) 5023, http://dx.doi.org/10.3390/ijms23095023.

[5] E. Deshayes, M. Roumiguie, C. Thibault, P. Beuzeboc, F. Cachin, C. Hennequin, D. Huglo, F. Rozet, D. Kassab-Chahmi, X. Rebillard, N. Houédé, Radium-223 dichloride for prostate cancer treatment, Drug Design Dev. Ther. 11 (2017) 2643–2651, http://dx.doi.org/10.2147/DDDT.S122417.

[6] R. Eychenne, M. Chérel, F. Haddad, F. Guérard, J.-F. Gestin, Overview of the most promising radionuclides for targeted alpha therapy: The "Hopeful Eight", Pharmaceutics 13 (2021) 906, http://dx.doi.org/10.3390/pharmaceutics13060906.

[7] C. Decristoforo, O. Neels, M. Patt, Emerging radionuclides in a regulatory framework for medicinal products–how do they fit? Front. Med. 8 (2021) 678452, http://dx.doi.org/10.3389/fmed.2021.678452.

[8] S.M. Qaim, I. Spahn, Development of novel radionuclides for medical applications, J. Label. Compounds Radiopharm. 61 (3) (2018) 126–140, http://dx.doi.org/10.1002/jlcr.3578.

[9] D.R. McAlister, E.P. Horwitz, Automated two column generator systems for medical radionuclides, Appl. Radiat. Isot. 67 (11) (2009) 1985–1991, http://dx.doi.org/10.1016/j.apradiso.2009.07.019.

[10] M.A. Synowiecki, L.R. Perk, J.F.W. Nijsen, Production of novel diagnostic radionuclides in small medical cyclotrons, EJNMMI Radiopharm. Chem. 3 (1) (2018) 1–25, http://dx.doi.org/10.1186/s41181-018-0038-z.

[11] P. Martini, A. Adamo, N. Syna, A. Boschi, L. Uccelli, N. Weeranoppanant, J. Markham, G. Pascali, Perspectives on the use of liquid extraction for radioisotope purification, Molecules 24 (2) (2019) 334, http://dx.doi.org/10.3390/molecules24020334.

[12] T. Mastren, V. Radchenko, A. Owens, R. Copping, R. Boll, J.R. Griswold, S. Mirzadeh, L.E. Wyant, M. Brugh, J.W. Engle, et al., Simultaneous separation of actinium and radium isotopes from a proton irradiated thorium matrix, Sci. Rep. 7 (1) (2017) 8216, http://dx.doi.org/10.1038/s41598-017-08506-9.

[13] V. Radchenko, J.W. Engle, J.J. Wilson, J.R. Maassen, F.M. Nortier, W.A. Taylor, E.R. Birnbaum, L.A. Hudston, K.D. John, M.E. Fassbender, Application of ion exchange and extraction chromatography to the separation of actinium from proton-irradiated thorium metal for analytical purposes, J. Chromatogr. A 1380 (2015) 55–63, http://dx.doi.org/10.1016/j.chroma.2014.12.045.

[14] A. Kotovskii, N. Nerozin, I. Prokof'ev, V. Shapovalov, Y.A. Yakovshchits, A. Bolonkin, A. Dunin, Isolation of actinium-225 for medical purposes, Radiochemistry 57 (2015) 285–291, http://dx.doi.org/10.1134/S1066362215030091.

[15] C. Rébufa, A. Traboulsi, V. Labed, N. Dupuy, M. Sergent, Experimental design approach for identification of the factors influencing the γ-radiolysis of ion exchange resins, Radiat. Phys. Chem. 106 (2015) 223–234, http://dx.doi.org/10.1016/j.radphyschem.2014.07.020.

[16] P. Wang, J. Zu, A. Khayambashi, R. Liu, Y. Wei, Gamma radiolysis of anion exchange resins based on 4-vinylpyridine in aqueous solution, J. Radioanal. Nucl. Chem. 311 (2017) 1619–1625, http://dx.doi.org/10.1007/s10967-016-5113-x.

[17] M. Aguilar, J.L. Cortina, Solvent Extraction and Liquid Membranes: Fundamentals and Applications in New Materials, CRC Press, 2008.

[18] H. Itabashi, T. Nakahara, Chelation solvent extraction for separation of metal ions, Compr. Anal. Chem. 41 (2003) 459–494, http://dx.doi.org/10.1016/S0166-526X(03)41015-5.

[19] M.F. Alam, Z.A. Begum, Y. Furusho, H. Hasegawa, I.M. Rahman, Selective separation of radionuclides from environmental matrices using proprietary solid-phase extraction systems: A review, Microchem. J. 181 (2022) 107637, http://dx.doi.org/10.1016/j.microc.2022.107637.

[20] N. Kabay, J.L. Cortina, A. Trochimczuk, M. Streat, Solvent-impregnated resins (SIRs)– Methods of preparation and their applications, React. Funct. Polym. 70 (8) (2010) 484–496, http://dx.doi.org/10.1016/j.reactfunctpolym.2010.01.005.

[21] A.M. Tamang, N. Singh, S.K. Chandraker, M.K. Ghosh, Solvent impregnated resin a potential alternative material for separation dyes, metal and phenolic compounds: A review, Curr. Res. Green Sustain. Chem. 5 (2021) 100232, http://dx.doi.org/10.1016/j.crgsc.2021.100232.

[22] A. Santoso, S. Trapp, V. van Steijn, R.M. de Kruijff, J.R. van Ommen, Method for preparing silicon elastomer beads loaded with chelating agents and their use for the separation of radionuclides, Netherlands Number: 2037212 (2024).

[23] J.N. Lee, C. Park, G.M. Whitesides, Solvent compatibility of poly (dimethylsiloxane)-based microfluidic devices, Anal. Chem. 75 (23) (2003) 6544–6554, http://dx.doi.org/10.1021/ac0346712.

[24] C. Rumens, M. Ziai, K. Belsey, J. Batchelor, S. Holder, Swelling of PDMS networks in solvent vapours; applications for passive RFID wireless sensors, J. Mater. Chem. C 3 (39) (2015) 10091–10098, http://dx.doi.org/10.1039/C5TC01927C.

[25] A. Trochimczuk, N. Kabay, M. Arda, M. Streat, Stabilization of solvent impregnated resins (SIRs) by coating with water soluble polymers and chemical crosslinking, React. Funct. Polym. 59 (1) (2004) 1–7, http://dx.doi.org/10.1016/j.reactfunctpolym.2003.12.011.

[26] S. Trapp, T. Lammers, E. Paulssen, R.M. de Kruijff, Rapid, automated radionuclide separation with high yield - towards microfluidic solvent extraction for ^{61,64,67}Cu production, in: European Research Reactor Conference, Antwerp, 2023, pp. 177–184.

[27] R. Chakravarty, N. Sen, S. Patra, A. Rajeswari, P. Shetty, K.K. Singh, S. Chakraborty, Microfluidic solvent extraction of no-carrier-added 64Cu from irradiated Zn target for radiopharmaceutical preparation, Chem. Eng. J. Adv. 13 (2023) 100433, http://dx.doi.org/10.1016/j.ceja.2022.100433.

[28] S. Trapp, T. Lammers, G. Engudar, C. Hoehr, A.G. Denkova, E. Paulssen, R.M. de Kruijff, Membrane-based microfluidic solvent extraction of Ga-68 from aqueous Zn solutions: towards an automated cyclotron production loop, EJNMMI Radiopharm. Chem. 8 (2023) 9, http://dx.doi.org/10.1186/s41181-023-00195-2.

[29] E. Oehlke, C. Hoehr, X. Hou, V. Hanemaayer, S. Zeisler, M.J. Adam, T.J. Ruth, A. Celler, K. Buckley, F. Benard, P. Schaffer, Production of Y-86 and other radiometals for research purposes using a solution target system, Nucl. Med. Biol. 42 (2015) 842–849, http://dx.doi.org/10.1016/j.nucmedbio.2015.06.005.

[30] R. Chakravarty, S. Patra, K. Jagadeesan, S. Thakare, S. Chakraborty, Electrochemical separation of 132/135-La theranostic pair from proton irradiated Ba target, Sep. Purif. Technol. 280 (2022) 119908, http://dx.doi.org/10.1016/j.seppur.2021.119908.

[31] C. Kratochwil, F. Bruchertseifer, F.L. Giesel, M. Weis, F.A. Verburg, F. Mottaghy, K. Kopka, C. Apostolidis, U. Haberkorn, A. Morgenstern, ^{225}Ac-PSMA-617 for PSMA-targeted alpha-radiation therapy of metastatic castration-resistant prostate cancer, J. Nucl. Med. 57 (2016) 1941–1944, http://dx.doi.org/10.2967/jnumed.116.178673.

[32] J.W. Engle, The production of Ac-225, Curr. Radiopharm. 11 (2018) 173–179, http://dx.doi.org/10.2174/1874471011666180418141357.

[33] U. Priyadarshini, S. Tandon, Spectrophotometric determination of vanadium (V) with N-benzoyl-N-phenylhydroxylamine, Anal. Chem. 33 (3) (1961) 435–438, http://dx.doi.org/10.1021/ac60171a040.

[34] R.J. Aguado, A. Mazega, N. Fiol, Q. Tarrés, P. Mutjé, M. Delgado-Aguilar, Durable nanocellulose-stabilized emulsions of dithizone/chloroform in water for Hg^{2+} detection: A novel approach for a classical problem, ACS Appl. Mater. Interfaces 15 (9) (2023) 12580–12589, http://dx.doi.org/10.1021/acsami.2c22713.

[35] K.K. Singh, S.K. Pathak, M. Kumar, A. Mahtele, S. Tripathi, P.N. Bajaj, Study of uranium sorption using D2EHPA-impregnated polymeric beads, J. Appl. Polym. Sci. 130 (5) (2013) 3355–3364, http://dx.doi.org/10.1002/app.39582.

[36] M.D. Abràmoff, P.J. Magalhães, S.J. Ram, Image processing with ImageJ, Biophotonics Int. 11 (7) (2004) 36–42.

[37] T. Church, Problems associated with the use of the ratio of Martin's diameter to Feret's diameter as a profile shape factor, Powder Technol. 2 (1) (1968) 27–31, http://dx.doi.org/10.1016/0032-5910(68)80030-0.

[38] J.P. Lewicki, J.J. Liggat, M. Patel, The thermal degradation behaviour of polydimethylsiloxane/montmorillonite nanocomposites, Polym. Degrad. Stab. 94 (9) (2009) 1548–1557, http://dx.doi.org/10.1016/j.polymdegradstab.2009.04.030.

[39] R.A. Meyer, J.F. Hazel, W.M. McNabb, Thermal analysis of some metal N-benzoyl-N-phenylhydroxylamine chelates, Anal. Chim. Acta 31 (1964) 419–425, http://dx.doi.org/10.1016/S0003-2670(00)88850-9.

[40] C.F. Croft, M.I.G. Almeida, S.D. Kolev, Characterisation of micro polymer inclusion beads by thermogravimetric analysis, Polymer 283 (2023) 126203, http://dx.doi.org/10.1016/j.polymer.2023.126203.

[41] N.H. Aprilita, M. Luqman, A. Suratman, Removal of cobalt (II) by dithizone-immobilized nickel slag, Results Chem. 5 (2023) 100698, http://dx.doi.org/10.1016/j.rechem.2022.100698.

[42] J. Cai, D. Xu, Z. Dong, X. Yu, Y. Yang, S.W. Banks, A.V. Bridgwater, Processing thermogravimetric analysis data for isoconversional kinetic analysis of lignocellulosic biomass pyrolysis: Case study of corn stalk, Renew. Sustain. Energy Rev. 82 (2018) 2705–2715, http://dx.doi.org/10.1016/j.rser.2017.09.113.

[43] A. Santoso, A. Damen, J.R. van Ommen, V. van Steijn, Atmospheric pressure atomic layer deposition to increase organic solvent resistance of PDMS, Chem. Commun. 58 (77) (2022) 10805–10808, http://dx.doi.org/10.1039/D2CC02402K.

[44] Y. Zhang, Z. Chen, Y. Shi, Q. Ma, H. Mao, Y. Li, H. Wang, Y. Zhang, Revealing the sorption mechanisms of carbamazepine on pristine and aged microplastics with extended DLVO theory, Sci. Total Environ. 874 (2023) 162480, http://dx.doi.org/10.1016/j.scitotenv.2023.162480.

[45] S.-L. Badea, S. Lundstedt, P. Liljelind, M. Tysklind, The influence of soil composition on the leachability of selected hydrophobic organic compounds (HOCs) from soils using a batch leaching test, J. Hazard. Mater. 254 (2013) 26–35, http://dx.doi.org/10.1016/j.jhazmat.2013.03.019.

[46] Y. Suo, Y. Ren, Research on the mechanism of nanofiltration membrane fouling in zero discharge process of high salty wastewater from coal chemical industry, Chem. Eng. Sci. 245 (2021) 116810, http://dx.doi.org/10.1016/j.ces.2021.116810.

[47] J.N. Israelachvili, Surface forces, in: The Handbook of Surface Imaging and Visualization, CRC Press, 2022, pp. 793–816.

[48] N.A. Mishchuk, The model of hydrophobic attraction in the framework of classical DLVO forces, Adv. Colloid Interface Sci. 168 (1–2) (2011) 149–166, http://dx.doi.org/10.1016/j.cis.2011.06.003.

[49] X. Liu, J. Xu, Y. Zhao, H. Shi, C.-H. Huang, Hydrophobic sorption behaviors of 17β-estradiol on environmental microplastics, Chemosphere 226 (2019) 726–735, http://dx.doi.org/10.1016/j.chemosphere.2019.03.162.

[50] O. Artiushenko, E.P. Avila, M. Nazarkovsky, V. Zaitsev, Reusable hydroxamate immobilized silica adsorbent for dispersive solid phase extraction and separation of rare earth metal ions, Sep. Purif. Technol. 231 (2020) 115934, http://dx.doi.org/10.1016/j.seppur.2019.115934.

[51] P. Sharma, K.H. Rao, Adhesion of paenibacillus polymyxa on chalcopyrite and pyrite: surface thermodynamics and extended DLVO theory, Colloids Surf. B 29 (1) (2003) 21–38, http://dx.doi.org/10.1016/S0927-7765(02)00180-7.

[52] H.H. Coenen, A.D. Gee, M. Adam, G. Antoni, C.S. Cutler, Y. Fujibayashi, J.M. Jeong, R.H. Mach, T.L. Mindt, V.W. Pike, A.D. Windhorst, Consensus nomenclature rules for radiopharmaceutical chemistry — Setting the record straight, Nucl. Med. Biol. 55 (2017) v–xi, http://dx.doi.org/10.1016/j.nucmedbio.2017.09.004.

[53] C.F. Ramogida, A.K. Robertson, U. Jermilova, C. Zhang, H. Yang, P. Kunz, J. Lassen, I. Bratanovic, V. Brown, L. Southcott, C. Rodríguez-Rodríguez, V. Radchenko, F. Bénard, C. Orvig, P. Schaffer, Evaluation of polydentate picolinic acid chelating ligands and an α-melanocyte-stimulating hormone derivative for targeted alpha therapy using ISOL-produced ^{225}Ac, EJNMMI Radiopharm. Chem. 4 (2019) http://dx.doi.org/10.1186/s41181-019-0072-5.

[54] M. Mudasir, R.A. Baskara, A. Suratman, K.S. Yunita, R. Perdana, W. Puspitasari, Simultaneous adsorption of Zn (II) and hg (II) ions on selective adsorbent of dithizone-immobilized bentonite in the presence of Mg (II) ion, J. Environ. Chem. Eng. 8 (4) (2020) 104002, http://dx.doi.org/10.1016/j.jece.2020.104002.

[55] H.B. Soltane, D. Roizard, E. Favre, Effect of pressure on the swelling and fluxes of dense PDMS membranes in nanofiltration: An experimental study, J. Membr. Sci. 435 (2013) 110–119, http://dx.doi.org/10.1016/j.memsci.2013.01.053.

[56] S. Batra, A. Awasthi, M. Iqbal, D. Datta, Solvent impregnated resins for the treatment of aqueous solutions containing different compounds: a review, Rev. Chem. Eng. 38 (2) (2022) 209–242, http://dx.doi.org/10.1515/revce-2019-0025.

[57] Y.H. Choi, K.H. Chung, H.B. Hong, W.S. Lee, Production of PDMS microparticles by emulsification of two phases and their potential biological application, Int. J. Polymeric Mater. Polymeric Biomater. 67 (11) (2018) 686–692, http://dx.doi.org/10.1080/00914037.2017.1375494.

[58] O. Dufaud, E. Favre, V. Sadtler, Porous elastomeric beads from crosslinked emulsions, J. Appl. Polym. Sci. 83 (5) (2002) 967–971, http://dx.doi.org/10.1002/app.2276.

[59] G. Zhang, D. Chen, W. Zhao, H. Zhao, L. Wang, W. Wang, T. Qi, A novel D2EHPA-based synergistic extraction system for the recovery of chromium(III), Chem. Eng. J. 302 (2016) 233–238, http://dx.doi.org/10.1016/j.cej.2016.05.063.

[60] B. Saha, K. Venkatesan, R. Natarajan, M. Antony, P. Vasudeva Rao, Studies on the extraction of uranium by N-octanoyl-N-phenylhydroxamic acid, Radiochim. Acta 90 (8) (2002) 455–459, http://dx.doi.org/10.1524/ract.2002.90.8_2002.455.

[61] X. Guo, B. Hurley, F. Yang, R. Buchheit, A novel organic conversion coating based on N-benzoyl-N-phenylhydroxylamine chemistry for the corrosion protection of AA2024-T3, Electrochim. Acta 246 (2017) 197–207, http://dx.doi.org/10.1016/j.electacta.2017.06.049.

[62] H. Tavallali, G. Deilamy-Rad, A. Parhami, S. Kiyani, Dithizone as novel and efficient chromogenic probe for cyanide detection in aqueous media through nucleophilic addition into diazenylthione moiety, Spectrochim Acta A 121 (2014) 139–146, http://dx.doi.org/10.1016/j.saa.2013.10.083.

[63] C.J. Van Oss, Interfacial Forces in Aqueous Media, CRC Press, 2006, http://dx.doi.org/10.1201/9781420015768.

[64] A.M. Smith, M. Borkovec, G. Trefalt, Forces between solid surfaces in aqueous electrolyte solutions, Adv. Colloid Interface Sci. 275 (2020) 102078, http://dx.doi.org/10.1016/j.cis.2019.102078.

[65] B. Mustin, B. Stoeber, Single layer deposition of polystyrene particles onto planar polydimethylsiloxane substrates, Langmuir 32 (1) (2016) 88–101, http://dx.doi.org/10.1021/acs.langmuir.5b02914.

[66] M.J. Bower, T.L. Bank, R.F. Giese, C.J. van Oss, Nanoscale forces of interaction between glass in aqueous and non-aqueous media: A theoretical and empirical study, Colloids Surf. A 362 (1–3) (2010) 90–96, http://dx.doi.org/10.1016/j.colsurfa.2010.03.040.

[67] K. Fazle Rabbi, J.Y. Ho, X. Yan, J. Ma, M.J. Hoque, S. Sett, N. Miljkovic, Polydimethylsiloxane-silane synergy enables dropwise condensation of low surface tension liquids, Adv. Funct. Mater. 32 (19) (2022) 2112837, http://dx.doi.org/10.1002/adfm.202112837.

[68] S. Vlassov, S. Oras, M. Antsov, I. Sosnin, B. Polyakov, A. Shutka, M.Y. Krauchanka, L.M. Dorogin, Adhesion and mechanical properties of PDMS-based materials probed with AFM: A review, Rev. Adv. Mater. Sci. 56 (1) (2018) 62–78, http://dx.doi.org/10.1515/rams-2018-0038.

[69] S.H. Donaldson Jr., J.P. Jahnke, R.J. Messinger, Å. Ostlund, D. Uhrig, J.N. Israelachvili, B.F. Chmelka, Correlated diffusivities, solubilities, and hydrophobic interactions in ternary polydimethylsiloxane–water–tetrahydrofuran mixtures, Macromolecules 49 (18) (2016) 6910–6917, http://dx.doi.org/10.1021/acs.macromol.6b01514.

[70] S.H. Donaldson Jr., A. Røyne, K. Kristiansen, M.V. Rapp, S. Das, M.A. Gebbie, D.W. Lee, P. Stock, M. Valtiner, J. Israelachvili, Developing a general interaction potential for hydrophobic and hydrophilic interactions, Langmuir 31 (7) (2015) 2051–2064, http://dx.doi.org/10.1021/la502115g.

[71] J. Chen, Q. Peng, X. Peng, H. Zhang, H. Zeng, Probing and manipulating noncovalent interactions in functional polymeric systems, Chem. Rev. 122 (18) (2022) 14594–14678, http://dx.doi.org/10.1021/acs.chemrev.2c00215.

[72] B.W. Ninham, On progress in forces since the DLVO theory, Adv. Colloid Interface Sci. 83 (1–3) (1999) 1–17, http://dx.doi.org/10.1016/S0001-8686(99)00008-1.

[73] Y. Fu, F. Hu, H. Li, L. Cui, G. Qian, D. Zhang, Y. Xu, Application and mechanisms of microalgae harvesting by magnetic nanoparticles (MNPs), Sep. Purif. Technol. 265 (2021) 118519, http://dx.doi.org/10.1016/j.seppur.2021.118519.

[74] J. Xu, L. Wang, H. Sun, Adsorption of neutral organic compounds on polar and nonpolar microplastics: Prediction and insight into mechanisms based on pp-LFERs, J. Hazard. Mater. 408 (2021) 124857, http://dx.doi.org/10.1016/j.jhazmat.2020.124857.

[75] M.C. Bridoux, H. Malandain, F. Leprince, F. Progent, X. Machuron-Mandard, Quantitative analysis of phosphoric acid esters in aqueous samples by isotope dilution stir-bar sorptive extraction combined with direct analysis in real time (DART)-Orbitrap mass spectrometry, Anal. Chim. Acta 869 (2015) 1–10, http://dx.doi.org/10.1016/j.aca.2015.01.010.

[76] H. Akaiwa, H. Kawamoto, The partition of dithizone between carbon tetrachloride and aqueous sulphuric acid, J. Inorg. Nucl. Chem. 29 (2) (1967) 541–545, http://dx.doi.org/10.1016/0022-1902(67)80059-9.

[77] I.P. Alimarin, F.P. Sudakov, B. Golovkin, Use of N-benzoyl-N-phenylhydroxylamine in analytical chemistry, Russ. Chem. Rev. 31 (8) (1962) 466, http://dx.doi.org/10.1070/RC1962v031n08ABEH001306.

[78] E. Monazam, R. Siriwardane, D. Miller, D. McIntyre, Rate analysis of sorption of Ce3+, Sm3+, and Yb3+ ions from aqueous solution using Dowex 50W-X8 as a sorbent in a continuous flow reactor, J. Rare Earths 36 (2018) 648–655, http://dx.doi.org/10.1016/j.jre.2017.10.010.

[79] M.A. Momen, M.L. Dietz, High-capacity extraction chromatographic materials based on polysulfone microcapsules for the separation and preconcentration of lanthanides from aqueous solution, Talanta 197 (2019) 612–621, http://dx.doi.org/10.1016/j.talanta.2019.01.026.

[80] A.M.S. El-Din, H.E. Rizk, E.H. Borai, E.S.M.E. Afifi, Selective separation and purification of cerium (III) from concentrate liquor associated with monazite processing by cationic exchange resin as adsorbent, Chem. Pap. 77 (2023) 2525–2538, http://dx.doi.org/10.1007/s11696-022-02643-w.

[81] W. Liu, Y. Zhang, S. Wang, L. Bai, Y. Deng, J. Tao, Effect of pore size distribution and amination on adsorption capacities of polymeric adsorbents, Molecules 26 (2021) 5267, http://dx.doi.org/10.3390/molecules26175267.

[82] D. Chapman, Electronegativity and the stability of metal complexes, Nature 174 (1954) 887–888, http://dx.doi.org/10.1038/174887a0.

[83] A. Mishustin, Estimate of the stability constants of trivalent actinide and lanthanide complexes with O-donor ligands in aqueous solutions, Russ. J. Inorg. Chem. 55 (2010) 746–752, http://dx.doi.org/10.1134/S0036023610050141.

[84] J. Fitzsimmons, B. Foley, B. Torre, M. Wilken, C.S. Cutler, L. Mausner, D. Medvedev, Optimization of cation exchange for the separation of actinium-225 from radioactive thorium, radium-223 and other metals, Molecules 24 (2019) 1921, http://dx.doi.org/10.3390/molecules24101921.

[85] S. Davern, D. O'Neil, H. Hallikainen, K. O'Neil, S. Allman, L. Millet, S. Retterer, M. Doktycz, R. Standaert, R. Boll, S.V. Cleve, D. DePaoli, S. Mirzadeh, Microfluidics-based separation of actinium-225 from radium-225 for medical applications, Sep. Sci. Technol. 54 (2019) 1994–2002, http://dx.doi.org/10.1080/01496395.2019.1614956.

[86] A.K.H. Robertson, C.F. Ramogida, P. Schaffer, V. Radchenko, Development of Ac-225 radiopharmaceuticals: TRIUMF perspectives and experiences, Curr. Radiopharm. 11 (2018) 156–172, http://dx.doi.org/10.2174/1874471011666180416161908.

[87] B. Zielinska, C. Apostolidis, F. Bruchertseifer, A. Morgenstern, An improved method for the production of Ac-225/Bi-213 from Th-229 for targeted alpha therapy, Solvent Extr. Ion Exch. 25 (2007) 339–349, http://dx.doi.org/10.1080/07366290701285108.

[88] M.T. Friend, T.G. Parker, T. Mastren, V. Mocko, M. Brugh, E.R. Birnbaum, M.E. Fassbender, Extraction chromatography of ^{225}Ac and lanthanides on N, N-dioctyldiglycolamic acid/1-butyl-3-methylimidazolium bis (trifluoromethylsulfonyl) imide solvent impregnated resin, J. Chromatogr. A 1624 (2020) 461219, http://dx.doi.org/10.1016/j.chroma.2020.461219.

[89] A. Baidak, J.A. LaVerne, Radiation-induced decomposition of anion exchange resins, J. Nucl. Mater. 407 (3) (2010) 211–219, http://dx.doi.org/10.1016/j.jnucmat.2010.10.025.

[90] C. Venkateswara Rao, A. Rout, S. Mishra, K. Venkatesan, Thermophysical properties of neat and radiolytically degraded acidic extractants present in room temperature ionic liquid, J. Radioanal. Nucl. Chem. 321 (2019) 907–916, http://dx.doi.org/10.1007/s10967-019-06648-w.

[91] I. Pucić, I. Cetina, A. Šantić, Component compatibility influences radiation stability of low temperature cured gels based on PDMS, Radiat. Phys. Chem. 185 (2021) 109493, http://dx.doi.org/10.1016/j.radphyschem.2021.109493.